

# PION WAVE FUNCTIONS FROM HOLOGRAPHIC QCD AND THE ROLE OF INFRARED RENORMALONS IN PHOTON-PHOTON COLLISIONS

A. I. Ahmadov<sup>1,2</sup> \*, C. Aydin<sup>1</sup> †, and F. Keskin<sup>1</sup> ‡

<sup>1</sup> *Department of Physics, Karadeniz Technical University, 61080, Trabzon, Turkey*

<sup>2</sup> *Department of Theoretical Physics, Baku State University,*

*Z. Khalilov st. 23, AZ-1148, Baku, Azerbaijan*

(Dated: December 6, 2018)

## Abstract

In this article, we calculate the contribution of the higher-twist Feynman diagrams to the large- $p_T$  inclusive single pion production cross section in photon-photon collisions in case of the running coupling and frozen coupling approaches within holographic QCD. We compare the resummed higher-twist cross sections with the ones obtained in the framework of the frozen coupling approach and leading-twist cross section. Also, we show that in the context of frozen coupling approach a higher-twist contribution to the photon-photon collisions cross section is normalized in terms of the pion electromagnetic form factor.

PACS numbers: 12.38.-t, 13.60.Le, 13.87.Fh,

Keywords: higher-twist, holographic QCD, infrared renormalons

---

\* E-mail: ahmadovazar@yahoo.com

† E-mail: coskun@ktu.edu.tr

‡ E-mail: feridunkeskin@ktu.edu.tr

## I. INTRODUCTION

One of the most significant theoretical advances in recent years has been the application of the AdS/CFT correspondence [1] between string theories defined in five-dimensional anti-de Sitter (AdS) space-time and conformal field theories in physical space-time. Quantum chromodynamics (QCD) is not itself a conformal theory; however there are indications, both from theory [2, 3] and phenomenology [4, 5] that the QCD coupling is slowly varying at small momentum transfer. In addition, one can argue that if the gluon has a maximum wavelength or an effective mass [6] due to confinement, that gluonic vacuum polarization corrections and the  $\beta$ -function must vanish in the infrared. If there is a conformal window where the QCD coupling is large and approximately constant and quark masses can be neglected, then QCD resembles a conformal theory, thus motivating the application of AdS/QCD to QCD. So, even though QCD is not conformally invariant, one can use the mathematical representation of the conformal group in five-dimensional anti-de Sitter space to construct an analytic first approximation to the theory. The resulting AdS/QCD model gives accurate predictions for hadron spectroscopy and a description of the quark structure of mesons and baryons which has scale invariance and dimensional counting at short distances, together with color confinement at large distances.

The hadronic wave function in terms of quark and gluon degrees of freedom plays an important role in QCD process predictions. For example, knowledge of the wave function allows to calculate distribution amplitudes and structure functions or conversely these processes can give phenomenological restrictions on the wave functions.

In References [7–11] the higher-twist effects were calculated within the frozen coupling constant approach. In Ref. [12], it was noted that in perturbative QCD (pQCD) calculations, the argument of the running coupling constant in both renormalization and factorization scale  $Q^2$  should be taken as equal to the square of the momentum transfer of a hard gluon in a corresponding Feynman diagram. But defining in this way,  $\alpha_s(Q^2)$  suffers from infrared singularities.

The contribution of large orders of perturbation theory related to the so-called renormalons has been investigated by several authors, using in particular the method of Borel summation [13–17]. In the case of (QCD), the coefficients of perturbative expansions in the QCD coupling  $\alpha_s$  can increase dramatically even at low orders. This fact together with

the apparent freedom in the choice of renormalization scheme and renormalization scales, limits the predictive power of perturbative calculations, even in applications involving large momentum transfer, where  $\alpha_s$  is effectively small.

Investigation of the infrared renormalon effects in various inclusive and exclusive processes is one of the most important and interesting problems in the perturbative QCD. It is known that infrared renormalons are responsible for factorial growth of coefficients in perturbative series for the physical quantities. But, these divergent series can be resummed by means of the Borel transformation [13] and the principal value prescription [18] and effects of infrared renormalons can be taken into account by a scale-setting procedure  $\alpha_s(Q^2) \rightarrow \alpha_s(\exp(f(Q^2))Q^2)$  at the one-loop order results. Technically, all-order resummation of infrared renormalons corresponds to the calculation of the one-loop Feynman diagrams with the running coupling constant  $\alpha_s(-k^2)$  at the vertices identically equivalent to calculation of the same diagrams with nonzero gluon mass.

In this work, we apply the running coupling approach [19] in order to compute the effects of the infrared renormalons on the pion production in photon-photon collisions within holographic QCD. This approach was also employed previously [20–24] to calculate the inclusive meson production in photon-proton, proton-proton and photon-photon collisions.

Since experiments examining high- $p_T$  particle production in two-photon collisions have been improved, it becomes important to reassess the various contributions which arise in quantum chromodynamics. Also the experimental measurement of the inclusive charged pion production cross section is important for the photon-photon collisions program at the future International Linear Collider(ILC).

Therefore, the calculation and analysis of the higher-twist effects on the dependence of the pion wave function in single pion production at photon-photon collisions by the running coupling approach within holographic QCD are very interesting search points.

In this respect, the contribution of the higher-twist Feynman diagrams to a single meson production cross section in photon-photon collisions is computed by using various pion wave functions from holographic QCD. Also, the leading and resummed higher-twist contributions are estimated and compared to each other.

We organize the paper as the follows; In Section II, we provide some formulae for the calculation of the contributions of the higher twist and leading twist diagrams. In Section III, we present some formulae and analysis of the higher twist effects on the dependence of

the pion wave function by the running coupling constant approach, and in Section IV, the numerical results for the cross section and discussion for the dependence of the cross section on the pion wave functions are presented. Finally, some concluding remark are stated in Section V.

## II. HIGHER TWIST AND LEADING TWIST CONTRIBUTIONS TO INCLUSIVE REACTIONS

The higher-twist Feynman diagrams for the pion production in the photon-photon collision  $\gamma\gamma \rightarrow MX$  are shown in Fig.1(a). The amplitude for this subprocess can be found by means of the Brodsky-Lepage formula [25]

$$M(\hat{s}, \hat{t}) = \int_0^1 dx_1 \int_0^1 dx_2 \delta(1 - x_1 - x_2) \Phi_M(x_1, x_2, Q^2) T_H(\hat{s}, \hat{t}; x_1, x_2). \quad (2.1)$$

In Eq.(2.1),  $T_H$  is the sum of the graphs contributing to the hard-scattering part of the subprocess. The hard-scattering amplitude  $T_H(\hat{s}, \hat{t}; x_1, x_2)$  depends on a process and can be obtained in the framework of pQCD and represented as a series in the QCD running coupling constant  $\alpha_s(Q^2)$ . The light-cone momentum fractions  $x \equiv x_1, x_2 = 1 - x$  specify the fractional momenta carried by quark and antiquark in the Fock state. As higher-twist subprocess which contribute to  $\gamma\gamma \rightarrow \pi X$ , we take  $\gamma q \rightarrow Mq$ .

The Mandelstam invariant variables for subprocesses  $\gamma q \rightarrow Mq$  are defined as

$$\hat{s} = (p_1 + p_\gamma)^2, \quad \hat{t} = (p_\gamma - p_M)^2, \quad \hat{u} = (p_1 - p_M)^2. \quad (2.2)$$

We have aimed to calculate the pion production cross section and to fix the differences due to the use of various pion model wave functions. The asymptotic pion wave functions [26, 27] and the Vega-Schmidt-Branz-Gutsche-Lyubovitskij (VSBGL) [28] wave function predicted by AdS/QCD, and also the pQCD evolution [29] has the form:

$$\begin{aligned} \Phi_{asy}^{hol}(x) &= \frac{4}{\sqrt{3}\pi} f_\pi \sqrt{x(1-x)}, \\ \Phi_{VSBGL}^{hol}(x) &= \frac{A_1 k_1}{2\pi} \sqrt{x(1-x)} \exp\left(-\frac{m^2}{2k_1^2 x(1-x)}\right), \quad \Phi_{asy}^p(x) = \sqrt{3} f_\pi x(1-x) \end{aligned} \quad (2.3)$$

where  $f_\pi = 92.4 MeV$  is the pion decay constant.

We now incorporate the higher-twist subprocess  $\gamma q \rightarrow Mq$  into the full inclusive cross section. In this subprocess photon and the pion may be viewed as an effective current

striking the incoming quark line. Therefore, the complete cross section in formal analogy with deep-inelastic scattering, is written as

$$E \frac{d\sigma}{d^3p}(\gamma\gamma \rightarrow MX) = \frac{3}{\pi} \sum_{q\bar{q}} \int_0^1 dx \delta(\hat{s} + \hat{t} + \hat{u}) \hat{s} G_{q/\gamma}(x, -\hat{t}) \frac{d\sigma}{d\hat{t}}(\gamma q \rightarrow Mq) + (t \leftrightarrow u). \quad (2.4)$$

Here  $G_{q/\gamma}$  is the per color distribution function for a quark in a photon. The subprocess cross section for  $\pi, \rho_L$  and  $\rho_T$  production is

$$\frac{d\sigma}{d\hat{t}}(\gamma q \rightarrow Mq) = \begin{cases} \frac{8\pi^2\alpha_E C_F}{9} [D(\hat{s}, \hat{u})]^2 \frac{1}{\hat{s}^2(-\hat{t})} \left[ \frac{1}{\hat{s}^2} + \frac{1}{\hat{u}^2} \right], & M = \pi, \rho_L, \\ \frac{8\pi^2\alpha_E C_F}{9} [D(\hat{s}, \hat{u})]^2 \frac{8(-\hat{t})}{\hat{s}^4\hat{u}^2}, & M = \rho_T, \end{cases} \quad (2.5)$$

where

$$D(\hat{s}, \hat{u}) = e_1 \hat{t} I_\pi(Q_1^2) \alpha_s(Q_1^2) + e_2 \hat{u} I_\pi(Q_2^2) \alpha_s(Q_2^2), \quad (2.6)$$

$$I_\pi(Q^2) = \int_0^1 dx \left[ \frac{\Phi_\pi(x, Q^2)}{x(1-x)} \right] \quad (2.7)$$

and  $Q_1^2 = \hat{s}/2$ ,  $Q_2^2 = -\hat{u}/2$ , represents the momentum squared carried by the hard gluon in Fig.1(a),  $e_1(e_2)$  is the charge of  $q_1(\bar{q}_2)$  and  $C_F = \frac{4}{3}$ .

The  $I_\pi$  factors reflect the exclusive form factor of the pion as is the motivation the arguments of  $\alpha_s$  and  $I_\pi$ . Note that the relation between  $I_\pi$  and the pion form factor completely fixes the normalization of the higher-twist subprocess. The full cross section for  $\pi$  and  $\rho_L$  production is given by

$$E \frac{d\sigma}{d^3p}(\gamma\gamma \rightarrow MX) = \frac{s}{s+u} \sum_{q\bar{q}} G_{q/\gamma}(x, -\hat{t}) \frac{8\pi\alpha_E C_F}{3} \frac{[D(\hat{s}, \hat{u})]^2}{\hat{s}^2(-\hat{t})} \left[ \frac{1}{\hat{s}^2} + \frac{1}{\hat{u}^2} \right] + \frac{s}{s+t} \sum_{q\bar{q}} G_{q/\gamma}(x, -\hat{u}) \frac{8\pi\alpha_E C_F}{3} \frac{[D(\hat{s}, \hat{t})]^2}{\hat{s}^2(-\hat{u})} \left[ \frac{1}{\hat{s}^2} + \frac{1}{\hat{t}^2} \right], \quad (2.8)$$

As seen from Eq.(2.8), the subprocess cross section for longitudinal  $\rho_L$  production is very similar to that for  $\pi$  production. We have extracted the following higher-twist subprocesses contributing to the two covariant cross sections in Eq.(2.5) as

$$\gamma q_1 \rightarrow (q_1 \bar{q}_2) q_2, \quad \gamma q_2 \rightarrow (q_1 \bar{q}_2) q_2. \quad (2.9)$$

Also from Eq.(2.8), at fixed  $p_T$ , the cross section falls very slowly with  $s$ . Additionally, at fixed  $s$ , the cross section decreases as  $1/p_T^5$ , multiplied by a slowly varying logarithmic

function which vanishes at the phase-space boundary. Thus, the  $p_T$  spectrum is fairly independent of  $s$  except near the kinematic limit.

One of the important problem in the single inclusive pion production in photon-photon collision is the possibility of normalization of the higher-twist subprocess cross section in terms of the electromagnetic form factor  $F_\pi(Q^2)$  of the pion. The electromagnetic form factor  $F_\pi(Q^2)$  of pion is given by the expression

$$F_\pi(Q^2) = \int_0^1 \int_0^1 dx_1 dx_2 \Phi_\pi^*(x_1, x_2, Q^2) T_H(x_1, x_2, \alpha_s(\lambda Q^2), Q^2) \Phi_\pi(x_1, x_2, Q^2). \quad (2.10)$$

This allows us to completely determine the  $\gamma q \rightarrow Mq$  cross section in terms of the pion form factor, through the relation

$$\frac{Q^2 F_\pi(Q^2)}{4\pi C_F \alpha_s(\hat{Q}^2)} = I_\pi^2(\hat{Q}^2) \quad (2.11)$$

It should be noted from Eq.(2.11) that the form factor contains the square of  $I_\pi(\hat{Q}^2)$ . In principle, experimental measurement of  $F_\pi(Q^2)$  determines  $I_\pi$  and hence the  $\gamma q \rightarrow Mq$ . So one can determine the cross section of  $\gamma\gamma \rightarrow MX$  explicitly.

Now we can conclude that in the frozen coupling constant approach  $\pi$  meson production higher-twist cross section of  $\gamma\gamma \rightarrow MX$  is normalized in terms of the pion electromagnetic form factor.

Extracting the higher-twist corrections to the pion production cross section and a comparison of higher-twist corrections with leading-twist contributions are essential problems. The contribution from the leading-twist subprocess  $\gamma\gamma \rightarrow q\bar{q}$  is shown in Fig.1(b). The corresponding inclusive cross section for production of a meson  $M$  is given by

$$\left[ \frac{d\sigma}{d^3p} \right]_{\gamma\gamma \rightarrow MX} = \frac{3}{\pi} \sum_{q,\bar{q}} \int_0^1 \frac{dz}{z^2} \delta(\hat{s} + \hat{t} + \hat{u}) \hat{s} D_q^M(z, -\hat{t}) \frac{d\sigma}{d\hat{t}}(\gamma\gamma \rightarrow q\bar{q}) \quad (2.12)$$

where

$$\hat{s} = s, \quad \hat{t} = \frac{t}{z}, \quad \hat{u} = \frac{u}{z}.$$

Here  $s$ ,  $t$ , and  $u$  refer to the overall  $\gamma\gamma \rightarrow MX$  reaction.  $D_q^M(z, -\hat{t})$  represents the quark fragmentation function into a pion containing a quark of the same flavor. For  $\pi^+$  production we assume that  $D_{\pi^+/u} = D_{\pi^+/\bar{d}}$ . In the leading-twist subprocess, pion is indirectly emitted from the quark with fractional momentum  $z$ . The final form for the leading-twist contribution to the large- $p_T$  pion production cross section in the process  $\gamma\gamma \rightarrow MX$  is

$$\Sigma_M^{LT} \equiv E \frac{d\sigma}{d^3P} = \frac{3}{\pi} \sum_{q,\bar{q}} \int_0^1 \frac{dz}{z^2} \delta(\hat{s} + \hat{t} + \hat{u}) \hat{s} D_q^M(z, -\hat{t}) \frac{d\sigma}{d\hat{t}}(\gamma\gamma \rightarrow q\bar{q}) =$$

$$\frac{3}{\pi} \sum_{q,\bar{q}} \int_0^1 d\frac{1}{z} \delta(s + \frac{1}{z}(t+u)) \hat{s} D_q^M(z, -\hat{t}) \frac{d\sigma}{dt}(\gamma\gamma \rightarrow q\bar{q}) = \frac{34}{27} \alpha_E^2 \frac{1}{z} D_q^M(z) \frac{1}{\hat{s}^2} \left[ \frac{\hat{t}}{\hat{u}} + \frac{\hat{u}}{\hat{t}} \right] \quad (2.13)$$

The contributions from these leading-twist subprocesses strongly depend on some phenomenological factors, such as, quark and gluon distribution functions in meson and fragmentation functions of various constituents *etc.* We should note that  $D(z, -\hat{t})/z$  behaves as  $1/z^2$  when  $z \rightarrow 0$ . For the kinematic range considered in our numerical calculations,  $D(z, -\hat{t})/z$  increases even more rapidly. We obtain of the final cross section, Eq.(2.13), as follows: At fixed  $p_T$ , the cross section decreases with  $s$  asymptotically as  $1/s$ . At fixed  $s$ , the  $D(z, -\hat{t})$  function causes the cross section to decrease rapidly when  $p_T$  increases towards the phase-space boundary ( $z \rightarrow 1$ ). As  $s$  increases, the phase-space boundary moves to higher  $p_T$ , and the  $p_T$  distribution broadens.

### III. HIGHER TWIST EFFECTS WITHIN HOLOGRAPHIC QCD AND THE ROLE INFRARED RENORMALONS

The main problem in our investigation is the calculation of the integral in Eq.(2.6) by the running coupling constant approach within holographic QCD. It should be noted that, in the exclusive processes, the coupling constant  $\alpha_s$  runs not only due to loop integration, but also because of the integration in the process amplitude over the light-cone momentum fraction of hadron constituents. In this respect, the exclusive processes have two independent sources of power corrections to their characteristics. One of the loop integration and the second integration over the light-cone momentum fraction of hadron constituents. Therefore, it is worth noting that, the renormalization scale (argument of  $\alpha_s$ ) according to Fig.1(a) should be chosen to be equal to  $Q_1^2 = (1-x)\hat{s}$ , and  $Q_2^2 = -x\hat{u}$ . The integral in Eq.(2.6) takes the form in the framework of the running coupling approach

$$D(\mu_{R_0}^2) = \int_0^1 \frac{\alpha_s(\lambda\mu_{R_0}^2) \Phi_M(x, \mu_F^2) dx}{x(1-x)}. \quad (3.1)$$

The  $\alpha_s(\lambda\mu_{R_0}^2)$  has the infrared singularity at  $x \rightarrow 1$ , for  $\lambda = 1-x$  or  $x \rightarrow 0$ , for  $\lambda = x$  and so the integral (3.1) diverges. For the regularization of the integral, we express the running coupling at scaling variable  $\alpha_s(\lambda\mu_{R_0}^2)$  with the aid of the renormalization group equation in terms of the fixed one  $\alpha_s(Q^2)$ . The solution of renormalization group equation for the

running coupling  $\alpha \equiv \alpha_s/\pi$  has the form [18]

$$\frac{\alpha(\lambda)}{\alpha} = \left[ 1 + \alpha \frac{\beta_0}{4} \ln \lambda \right]^{-1}. \quad (3.2)$$

Then, for  $\alpha_s(\lambda Q^2)$ , we get

$$\alpha(\lambda Q^2) = \frac{\alpha_s}{1 + \ln \lambda/t} \quad (3.3)$$

where  $t = 4\pi/\alpha_s(Q^2)\beta_0 = 4/\alpha\beta_0$ .

Having inserted Eq.(3.3) into Eq.(2.6) we obtain

$$\begin{aligned} D(\hat{s}, \hat{u}) &= e_1 \hat{u} \int_0^1 dx \frac{\alpha_s(\lambda \mu_{R_0}^2) \Phi_M(x, Q_1^2)}{x(1-x)} + e_2 \hat{s} \int_0^1 dx \frac{\alpha_s(\lambda \mu_{R_0}^2) \Phi_M(x, Q_2^2)}{x(1-x)} \\ &= e_1 \hat{u} \alpha_s(\hat{s}) t_1 \int_0^1 dx \frac{\Phi_M(x, Q_1^2)}{x(1-x)(t_1 + \ln \lambda)} + e_2 \hat{s} \alpha_s(-\hat{u}) t_2 \int_0^1 dx \frac{\Phi_M(x, Q_2^2)}{x(1-x)(t_2 + \ln \lambda)} \end{aligned} \quad (3.4)$$

where  $t_1 = 4\pi/\alpha_s(\hat{s})\beta_0$  and  $t_2 = 4\pi/\alpha_s(-\hat{u})\beta_0$ .

Although the integral (3.4) is still divergent, it is recast into a suitable form for calculation.

Making the change of variable as  $z = \ln \lambda$ , we obtain

$$D(\hat{s}, \hat{u}) = e_1 \hat{u} \alpha_s(\hat{s}) t_1 \int_0^1 \frac{\Phi_M(x, Q^2) dx}{x(1-x)(t_1 + z)} + e_2 \hat{s} \alpha_s(-\hat{u}) t_2 \int_0^1 \frac{\Phi_M(x, Q^2) dx}{x(1-x)(t_2 + z)} \quad (3.5)$$

In order to calculate (3.5), we will apply the integral representation of  $1/(t+z)$  [30, 31] as

$$\frac{1}{t+z} = \int_0^\infty e^{-(t+z)u} du \quad (3.6)$$

which gives

$$D(\hat{s}, \hat{u}) = e_1 \hat{t} \alpha_s(\hat{s}) t_1 \int_0^1 \int_0^\infty \frac{\Phi_\pi(x, Q_1^2) e^{-(t_1+z)u} du dx}{x(1-x)} + e_2 \hat{u} \alpha_s(-\hat{u}) t_2 \int_0^1 \int_0^\infty \frac{\Phi_\pi(x, Q_2^2) e^{-(t_2+z)u} du dx}{x(1-x)}. \quad (3.7)$$

In the case  $\Phi_{asy}^{hol}(x)$  for the  $D(\hat{s}, \hat{u})$ , Eq.(3.7) is written as

$$D(\hat{s}, \hat{u}) = \frac{16f_\pi e_1 \hat{u}}{\sqrt{3}\beta_0} \int_0^\infty du e^{-t_1 u} B\left(\frac{1}{2}, \frac{1}{2} - u\right) + \frac{16f_\pi e_2 \hat{s}}{\sqrt{3}\beta_0} \int_0^\infty du e^{-t_2 u} B\left(\frac{1}{2}, \frac{1}{2} - u\right) \quad (3.8)$$

and for  $\Phi_{asy}^p(x)$  wave function

$$D(\hat{s}, \hat{u}) = \frac{4\sqrt{3}\pi f_\pi e_1 \hat{u}}{\beta_0} \int_0^\infty du e^{-t_1 u} \left[ \frac{1}{1-u} \right] + \frac{4\sqrt{3}\pi f_\pi e_2 \hat{s}}{\beta_0} \int_0^\infty du e^{-t_2 u} \left[ \frac{1}{1-u} \right]. \quad (3.9)$$

where  $B(\alpha, \beta)$  is Beta function. The structure of the infrared renormalon poles in Eq.(3.8) and Eq.(3.9) strongly depend on the wave functions of the pion. To remove them from Eq.(3.8) and Eq.(3.9) we adopt the principal value prescription. We denote the higher-twist cross section obtained using the running coupling constant approach by  $(\Sigma_\pi^{HT})^{res}$ .

#### IV. NUMERICAL RESULTS AND DISCUSSION

In this section, we discuss the numerical results for higher-twist and renormalon effects with higher-twist contributions calculated in the context of the running coupling constant and frozen coupling approaches on the dependence of the chosen pion wave functions in the process  $\gamma\gamma \rightarrow MX$  within holographic QCD. For the higher-twist subprocess, we take  $\gamma q_1 \rightarrow (q_1 \bar{q}_2) q_2$ , and  $\gamma q_2 \rightarrow (q_1 \bar{q}_2) q_2$  contributing to  $\gamma\gamma \rightarrow MX$  cross sections. Inclusive pion photoproduction represents a significant test case in which higher-twist terms dominate those of leading-twist terms in certain kinematic domains. For the dominant leading-twist subprocess for the meson production, we take the photon-photon annihilation  $\gamma\gamma \rightarrow q\bar{q}$  in which the  $\pi$  pion is indirectly emitted from the quark. The quark distribution function inside the photon was used [32] and the gluon and quark fragmentation functions into a pion was used [33].

The results of our numerical calculations are plotted in Figs.2-15. Firstly, it is very interesting comparing the higher twist cross sections obtained within holographic QCD with the ones obtained within perturbative QCD. In Fig.2 and Fig.3 we show the dependence of higher-twist cross sections  $(\Sigma_{\pi^+}^{HT})^0$ , and  $(\Sigma_{\pi^+}^{HT})^{res}$  calculated in the context of the frozen and running coupling constant approaches as a function of the pion transverse momentum  $p_T$  for  $\Phi_{\pi}^{hol}(x)$ ,  $\Phi_{\pi}^p(x)$  and  $\Phi_{VSBGL}^{hol}(x)$  pion wave functions at  $y = 0$ . It is seen from the figures that the higher-twist cross section is monotonically decreasing with an increase in the transverse momentum of the pion. In Fig.4-Fig.7, we show the dependence of the ratios  $(\Sigma_{HT}^{hol})^0/(\Sigma_{\pi^+}^{HT})^0$ ,  $(\Sigma_{\pi^+}^{HT})^{res}/(\Sigma_{\pi^+}^{HT})^0$ ,  $(\Sigma_{\pi^+}^{HT})^0/(\Sigma_{\pi^+}^{LT})$  and  $(\Sigma_{\pi^+}^{HT})^{res}/(\Sigma_{\pi^+}^{LT})$  as a function of the pion transverse momentum  $p_T$  for  $\Phi_{\pi}^{hol}(x)$ ,  $\Phi_{\pi}^p(x)$  and  $\Phi_{VSBGL}^{hol}(x)$  pion wave functions. Here  $\Sigma_{\pi^+}^{LT}$  is the leading-twist cross section. As shown in Fig.4, in the region  $20 \text{ GeV}/c < p_T < 80 \text{ GeV}/c$  higher-twist cross section for  $\Phi_{\pi}^{hol}(x)$  is suppress by about half orders of magnitude relative to the higher-twist cross section for  $\Phi_{VSBGL}^{hol}(x)$ , but in the regions  $10 \text{ GeV}/c < p_T < 20 \text{ GeV}/c$  and  $80 \text{ GeV}/c < p_T < 90 \text{ GeV}/c$ , higher-twist cross section  $(\Sigma_{HT}^{hol})^0$  is suppress by about two orders of magnitude relative to the higher-twist cross section for  $(\Sigma_{VSBGL}^{hol})^0$ . Also higher-twist cross section for  $\Phi_{\pi}^p(x)$  is suppress by about half orders of magnitude relative to the higher-twist cross section for  $\Phi_{VSBGL}^{hol}(x)$ . In Fig.5, Fig.6 and Fig.7, the dependence of the ratios  $(\Sigma_{\pi}^{HT})^{res}/(\Sigma_{\pi^+}^{HT})^0$ ,  $(\Sigma_{\pi^+}^{HT})^0/(\Sigma_{\pi^+}^{LT})$  and  $(\Sigma_{\pi^+}^{HT})^{res}/(\Sigma_{\pi^+}^{LT})$  are displayed as a function of the pion transverse momentum  $p_T$  for the  $\Phi_{\pi}^{hol}(x)$ ,  $\Phi_{\pi}^p(x)$  and  $\Phi_{VSBGL}^{hol}(x)$  pion wave functions. It

is see that, resummed higher-twist cross section for  $\Phi_{asy}^{hol}(x)$  is suppress by about two orders of magnitude relative to the higher-twist cross section for  $(\Sigma_{VSBGL}^{hol})^0$ . Noticed that one-half order is suppress for  $(\Sigma_{asy}^{hol})^0$  and one order is suppress for  $(\Sigma_{asy}^p)^0$ . It is observed from Fig.6 and Fig.7 that, the ratios  $(\Sigma_{\pi^+}^{HT})^0/(\Sigma_{\pi^+}^{LT})$  and  $(\Sigma_{\pi^+}^{HT})^{res}/(\Sigma_{\pi^+}^{LT})$  for all wave functions decrease with an increase in the transverse momentum of pion. In Fig.8 - Fig.10, we have depicted higher-twist cross sections  $(\Sigma_{HT}^{hol})^0$ , and ratio  $(\Sigma_{HT}^{hol})^0/(\Sigma_{\pi^+}^{HT})^0$ ,  $(\Sigma_{HT}^{hol})^{res}/(\Sigma_{\pi^+}^{HT})^0$ , as a function of the rapidity  $y$  of the pion at  $\sqrt{s} = 183 \text{ GeV}$  and  $p_T = 14.6 \text{ GeV}/c$ . The figures show that the higher-twist cross section and ratios have a different distinctive behavior. As is seen in Fig.9 ratio  $(\Sigma_{asy}^{hol})^0/(\Sigma_{VSBGL}^{hol})^0$  has a maximum approximately at the point  $y = -1.92$ . However in this point ratio  $(\Sigma_{VSBGL}^{hol})^0/(\Sigma_{asy}^p)^0$  has a minimum. As is seen from Fig.10 resummed higher-twist cross section for  $\Phi_{asy}^{hol}(x)$  is suppress by about one order of magnitude relative to the resummed higher-twist cross section for  $\Phi_{asy}^p(x)$  and with an increasing rapidity of pion ratio is kepped approximately constant. But resummed higher-twist cross section for  $\Phi_{asy}^{hol}(x)$  is suppress by about one half- two orders of magnitude relative to the frozen higher-twist cross section for  $\Phi_{VSBGL}^{hol}(x)$  and has a maximum approximately at the point  $y = -1.92$ . However resummed higher-twist cross section for  $\Phi_{asy}^{hol}(x)$  is suppress by about one order of magnitude relative for resummed higher-twist cross section for  $\Phi_{asy}^p(x)$  and to stay is constant with an increasing rapidity of pion. Figures also show that, the ratio depends on the choice of the pion wave function. Analysis of our calculations concludes that  $(\Sigma_{\pi^+}^{HT})^0$ , and  $(\Sigma_{\pi^+}^{HT})^{res}$  higher-twist cross sections and ratio sensitive to pion wave functions predicted by holographic and perturbative QCD.

We have also carried out comparative calculations in the center-of-mass energy  $\sqrt{s} = 209 \text{ GeV}$  and obtained results are displayed in Fig.11-Fig.15. Analysis of our calculations at the center-of-mass energies  $\sqrt{s} = 183 \text{ GeV}$  and  $\sqrt{s} = 209 \text{ GeV}$ , show that with increasing in the beam energy contributions of higher twist effects to the cross section decrease by about 1-2 orders of magnitude. As is seen from Fig.4, Fig.5, Fig.9, Fig.10, Fig.12, Fig.14 and Fig.15 that infrared renormalon effects enhance the perturbative predictions for the pion production cross section in the photon-photon collisions about 1-2 orders of magnitude. Our opinion is this feature of infrared renormalons may help the explain theoretical interpretations with future experimental data for the pion production cross section in the photon-photon collisions. In our calculations of the higher-twist cross section of the process the dependence of the transverse momentum of pion appears in the range of  $(10^{-9} \div 10^{-22}) \text{ mb}/\text{GeV}^2$ . Therefore,

higher-twist cross section obtained in our work should be observable at ILC.

## V. CONCLUSIONS

In this work, the single meson inclusive production via higher twist mechanism within holographic QCD are calculated . For calculation of the cross section the running coupling constant approach is applied and infrared renormalon poles in the cross section expression are revealed. Infrared renormalon induced divergences is regularized by means of the principal value prescription and the Borel sum for the higher twist cross section is found. It is observed that, the resummed higher-twist cross section differs from that found using the frozen coupling approximation in some region considerably. We proved that the higher-twist cross section for  $\pi$  pion production in the photon-photon collisions may be normalized in terms of the pion form factor. The following results can be concluded from the experiments; the higher-twist contributions to single meson production cross section in the photon-photon collisions have important phenomenological consequences, the higher-twist pion production cross section in the photon-photon collisions depends on the form of the pion model wave functions and may be used for their study. Also that the contributions of renormalons effects within holographic QCD in this process is essential and may help to analyse experimental results. Further investigations are needed in order to clarify the role of higher-twist effects in QCD. Especially, the future ILC measurements will provide further tests of the dynamics of large- $p_T$  hadron production beyond the leading twist.

### Acknowledgments

One of author A.I.Ahmadov is grateful to all members of the Department of Physics of Karadeniz Technical University for appreciates hospitality extended to him in Trabzon. Financial support by TUBITAK under grant number 2221(Turkey) is also gratefully acknowledged.

- 
- [1] J. M. Maldacena, Adv. Theor. Math. Phys. **2**, 231 (1998) [Int. J. Theor. Phys. **38**, 1113 (1999); S. S. Gubser, I. R. Klebanov and A. M. Polyakov, Phys. Lett. **B428**, 105 (1998); E. Witten,

- Adv. Theor. Math. Phys. **2**, 253 (1998).
- [2] L. von Smekal, R. Alkofer and A. Hauck, Phys. Rev. Lett. **79**, 3591 (1997).
- [3] S.Furui and H. Nakajima, Phys.Rev. **D76**, 054509 (2007); Proc. Sci., LAT2007 (2007) 301 [arXiv:0708.1421].
- [4] S. J. Brodsky, S. Menke, C. Merino and J. Rathsman, Phys. Rev. **D67**, 055008 (2003).
- [5] A. Deur, V. Burkert, J. P. Chen and W. Korsch, Phys. Lett. **B650**, 244 (2007).
- [6] J. M. Cornwall, Phys. Rev. **D26**, 1453 (1982).
- [7] J. A. Bagger and J. F. Gunion, Phys. Rev. **D29**, 40 (1984).
- [8] A. Bagger and J. F. Gunion, Phys. Rev. **D25**, 2287 (1982).
- [9] A. I. Ahmadov, I. Boztosun, R. Kh. Muradov, A. Soylyu, and E. A. Dadashov, Int. J. Mod.Phys. **E15**, 1209 (2006).
- [10] A. I. Ahmadov, I. Boztosun, A. Soylyu, and E. A. Dadashov, Int. J. Mod.Phys. **E17**, 1041 (2008).
- [11] V. N. Baier and A. Grozin, Phys. Lett. **B96**, 181 (1980); S. Gupta, Phys. Rev. **D24**, 1169 (1981).
- [12] S. J. Brodsky, G.L. Lepage and P. B. Mackenzie, Phys. Rev. **D28**, 228 (1983).
- [13] G.'t. Hooft, in The Whys of Subnuclear Physics, Erice, 1977, edited by A. Zichichi (Plenum, New York, 1979), p.94
- [14] A. H. Mueller, Nucl. Phys. **B250**, 327 (1985); Phys. Lett. **B308**, 355 (1993).
- [15] V. I. Zakharov, Nucl. Phys. **B385**,452 (1992).
- [16] M. Beneke, Phys. Rep. **317**, 1 (1999).
- [17] W. Greiner, S. Schramm and E. Stein, Quantum Chromodynamics, 2nd edn.(Berlin, Springer, 2002), pp.551.
- [18] H. Contopanagos and G. Sterman, Nucl. Phys. **B419**, 77 (1994)
- [19] S.S. Agaev, Phys. Lett. **B360**, 117 (1995); **B369**, 379(E) (1996).
- [20] S.S. Agaev, Eur. Phys. J. **C1**, 321 (1998).
- [21] A. I. Ahmadov, Coskun Aydin, Sh. M. Nagiyev, Yilmaz A. Hakan, and E. A. Dadashov, Phys. Rev. **D80**, 016003 (2009).
- [22] A. I. Ahmadov, Coskun Aydin, E. A. Dadashov and Sh. M. Nagiyev, Phys. Rev. **D81**, 054016 (2010).
- [23] A. I. Ahmadov, R. M. Burjaliyev, Int. J. Mod. Phys. **E20**, 1243 (2011).

- [24] A. I. Ahmadov, Sh. M. Nagiyev and E. A. Dadashov , arxiv: hep-ph/1107.1562
- [25] G. L. Lepage and S. J. Brodsky, Phys. Rev. **D22**, 2157 (1980).
- [26] S. J. Brodsky and G. F. de Teramond, Phys. Rev. **D77**, 056007 (2008).
- [27] S. J. Brodsky, Proc. Sci.LHC07 (2007) 002 [arxiv:hep-ph/0707.2643] .
- [28] A. Vega, I. Schmidt, T. Branz, T.Gutsche,V. Lyubovitskij, Phys. Rev. **D80**, 055014 (2009).
- [29] G. P. Lepage and S. J. Brodsky, Phys.Lett. **B87**, 359 (1979).
- [30] J. Zinn-Justin, Phys. Rept. **70**, 109 (1981).
- [31] A. Erdelyi, Higher Transcendental Functions (McGrow-Hill Book Company, New York, 1953),  
Vol.2.
- [32] F. Cornet, Acta Phys. Polon. **B37**, 663 (2006).
- [33] S. Albino, B. A. Kniehl, G. Kramer, Nucl.Phys. **B725**, 181 (2005).

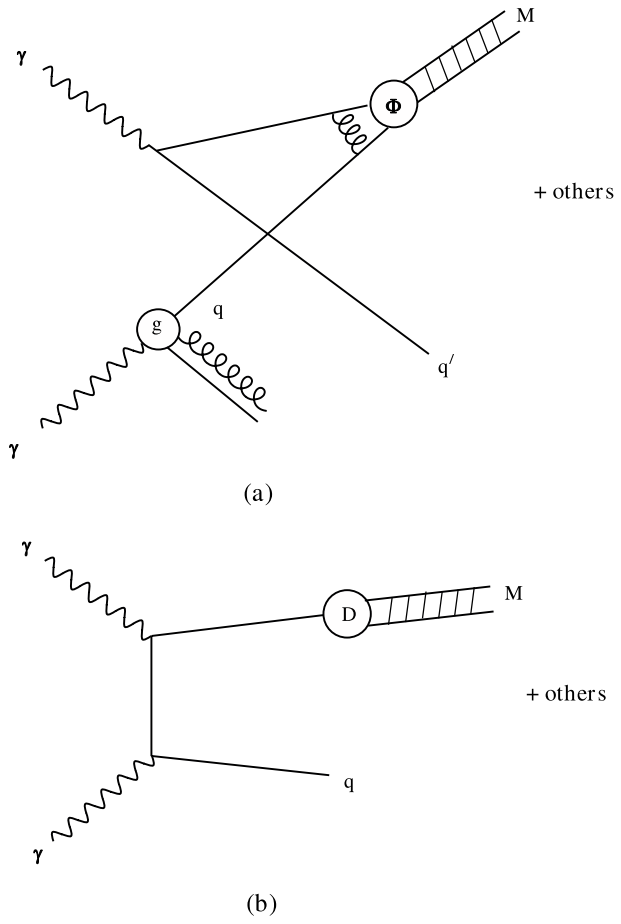


FIG. 1: (a): The higher-twist contribution to  $\gamma\gamma \rightarrow MX$ ; (b): The leading-twist contribution to  $\gamma\gamma \rightarrow MX$

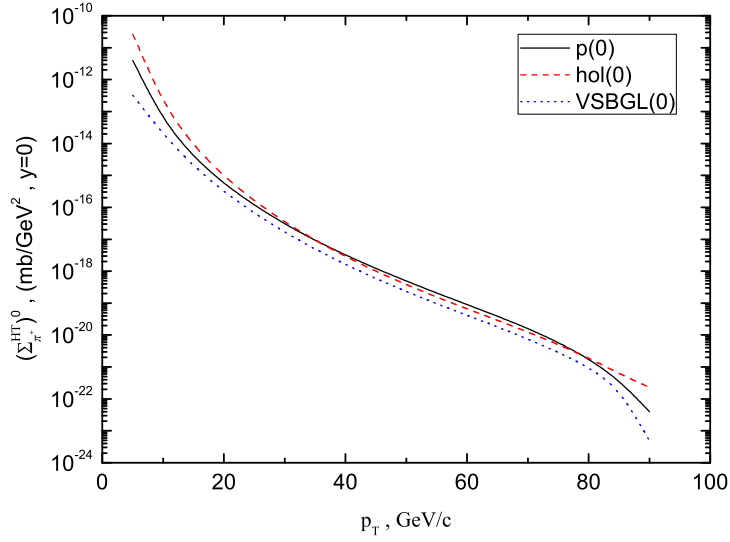


FIG. 2: Higher-twist  $\pi^+$  production cross section  $(\Sigma_{\pi^+}^{HT})^0$  as a function of the  $p_T$  transverse momentum of the pion at the c.m. energy  $\sqrt{s} = 183 \text{ GeV}$ .

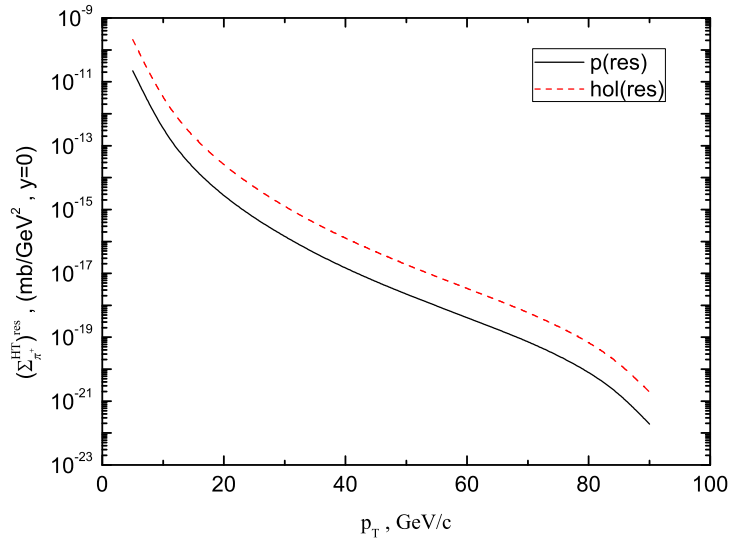


FIG. 3: Higher-twist  $\pi^+$  production cross section  $(\Sigma_{\pi^+}^{HT})^{res}$  as a function of the  $p_T$  transverse momentum of the pion at the c.m. energy  $\sqrt{s} = 183 \text{ GeV}$ .

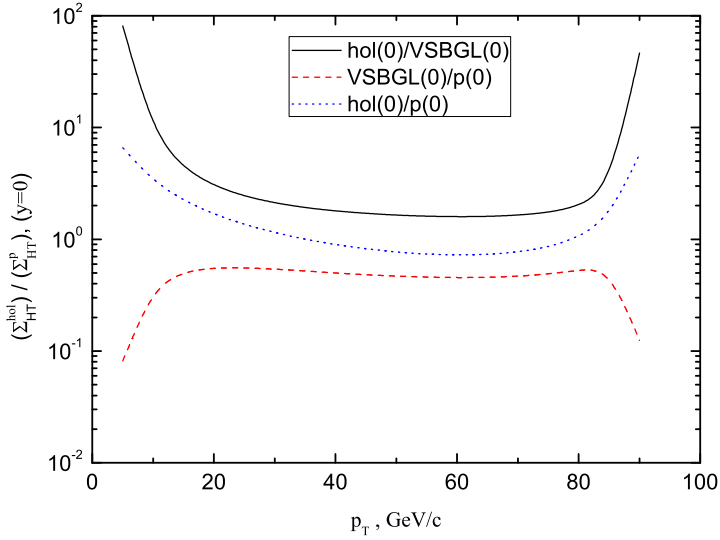


FIG. 4: Ratio  $(\Sigma_{HT}^{hol})^0 / (\Sigma_{\pi^+}^{HT})^0$ , where higher-twist contribution are calculated for the pion rapidity  $y = 0$  at the c.m.energy  $\sqrt{s} = 183 \text{ GeV}$  as a function of the pion transverse momentum,  $p_T$ .

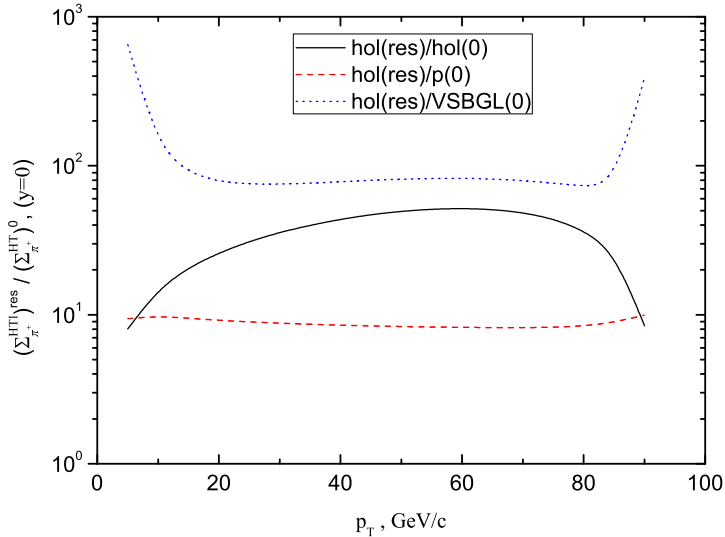


FIG. 5: Ratio  $(\Sigma_{HT}^{hol})^{res} / (\Sigma_{\pi^+}^{HT})^0$ , as a function of the  $p_T$  transverse momentum of the pion at the c.m. energy  $\sqrt{s} = 183 \text{ GeV}$ .

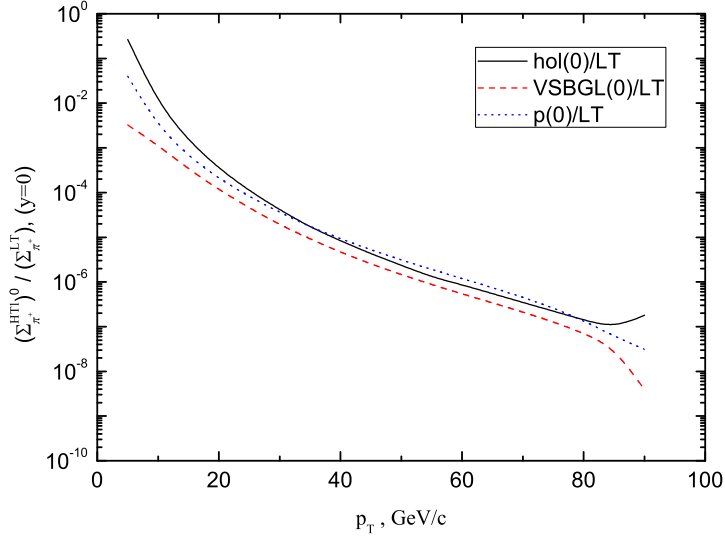


FIG. 6: Ratio  $(\Sigma_{\pi^+}^{HT})^0 / (\Sigma_{\pi^+}^{LT})$ , where higher-twist contribution are calculated for the pion rapidity  $y = 0$  at the c.m.energy  $\sqrt{s} = 183 \text{ GeV}$  as a function of the pion transverse momentum,  $p_T$ .

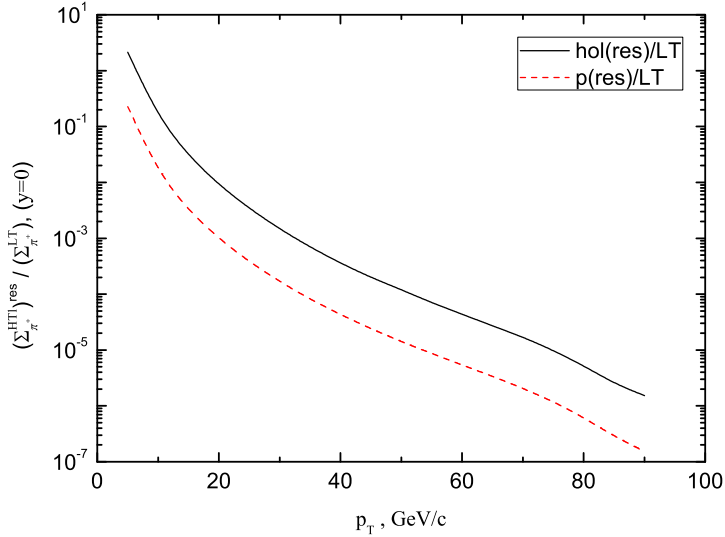


FIG. 7: Ratio  $(\Sigma_{\pi^+}^{HT})^{res} / (\Sigma_{\pi^+}^{LT})$ , as a function of the  $p_T$  transverse momentum of the pion at the c.m. energy  $\sqrt{s} = 183 \text{ GeV}$ .

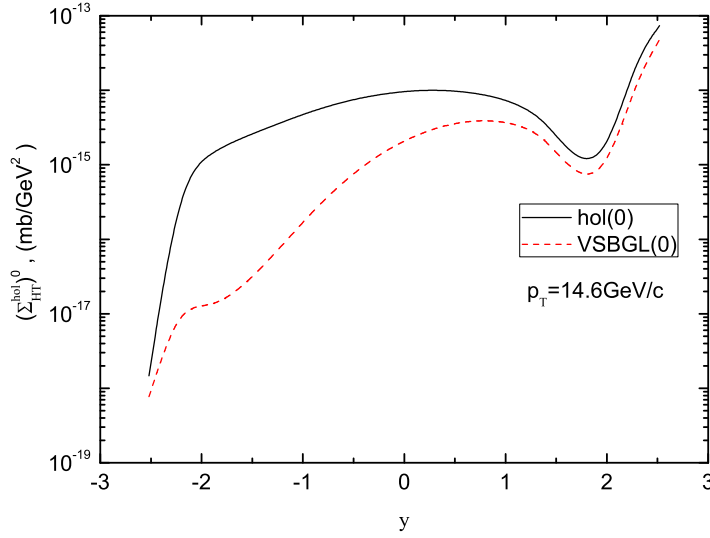


FIG. 8: Higher-twist  $\pi^+$  production cross section  $(\Sigma_{HT}^{hol})^0$ , as a function of the  $y$  rapidity of the pion at the transverse momentum of the pion  $p_T = 14.6 \text{ GeV}/c$ , at the c.m. energy  $\sqrt{s} = 183 \text{ GeV}$ .

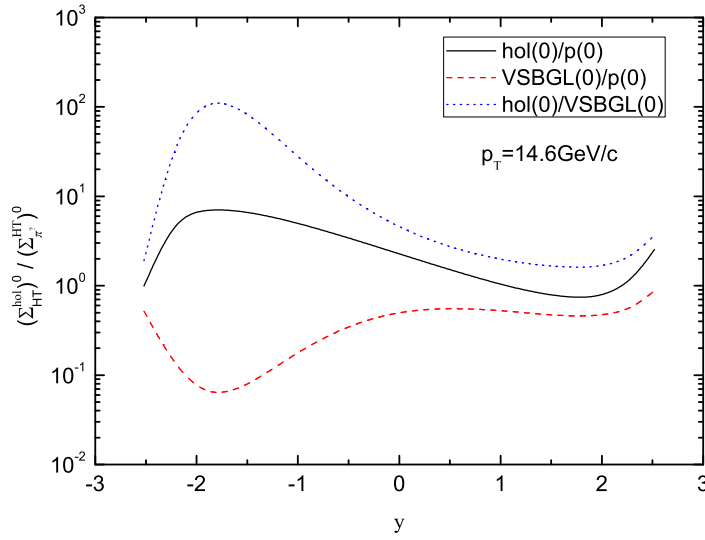


FIG. 9: Ratio  $(\Sigma_{HT}^{hol})^0 / (\Sigma_{\pi^+}^{HT})^0$ , as a function of the  $y$  rapidity of the pion at the transverse momentum of the pion  $p_T = 14.6 \text{ GeV}/c$ , at the c.m. energy  $\sqrt{s} = 183 \text{ GeV}$ .

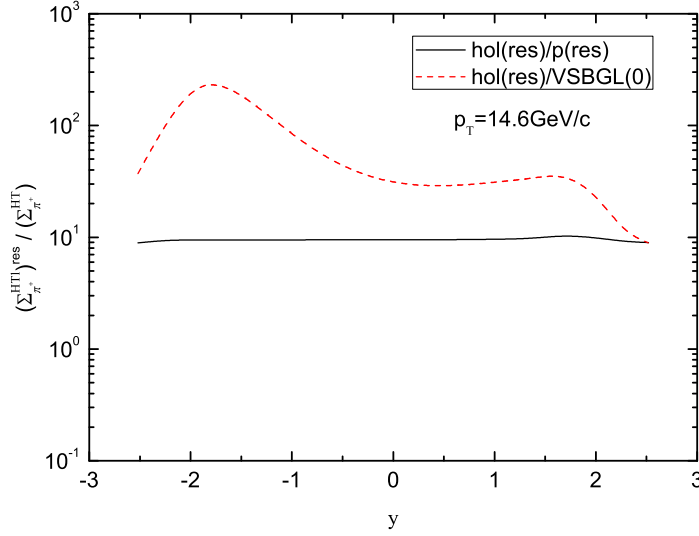


FIG. 10: Ratio  $(\Sigma_{\pi^+}^{HT})^{res}/(\Sigma_{\pi^+}^{HT})^0$ , as a function of the  $y$  rapidity of the pion at the transverse momentum of the pion  $p_T = 14.6 \text{ GeV}/c$ , at the c.m. energy  $\sqrt{s} = 183 \text{ GeV}$ .

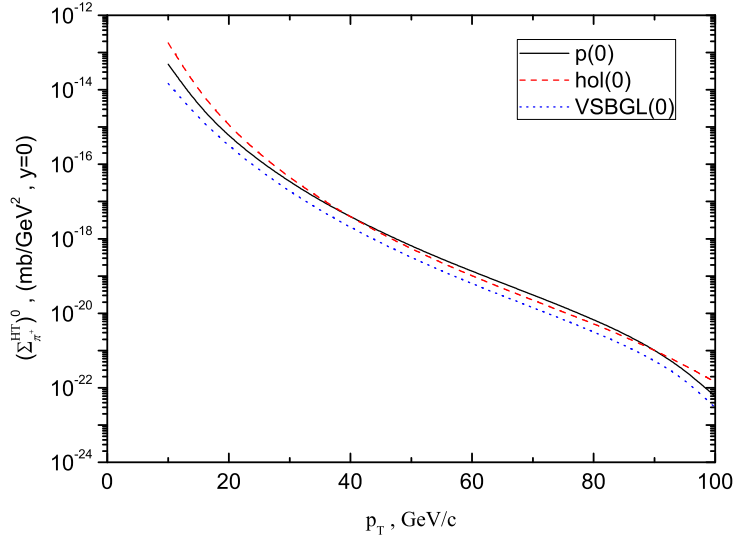


FIG. 11: Higher-twist  $\pi^+$  production cross section  $(\Sigma_{\pi^+}^{HT})^0$  as a function of the  $p_T$  transverse momentum of the pion at the c.m. energy  $\sqrt{s} = 209 \text{ GeV}$ .

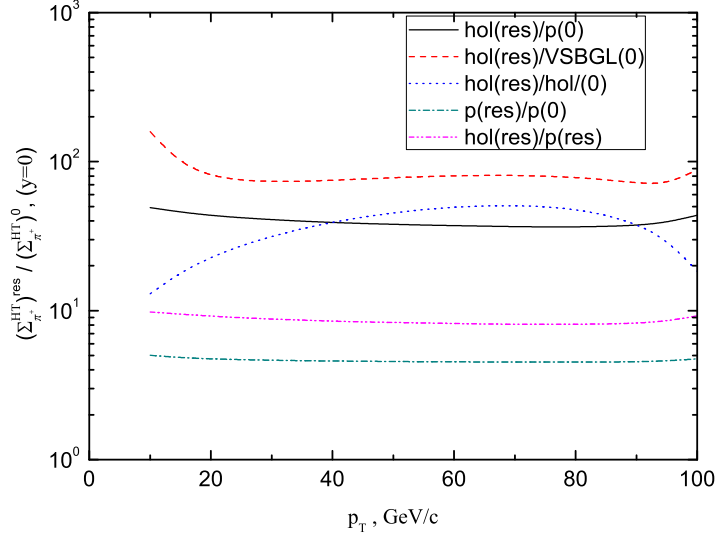


FIG. 12: Ratio  $(\Sigma_{HT}^{hol})^{res}/(\Sigma_{\pi^+}^{HT})^0$ , as a function of the  $p_T$  transverse momentum of the pion at the c.m. energy  $\sqrt{s} = 209 \text{ GeV}$ .

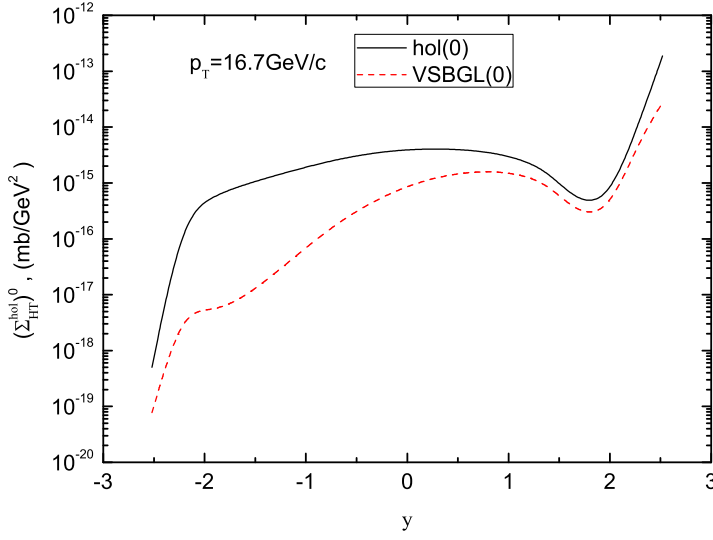


FIG. 13: Higher-twist  $\pi^+$  production cross section  $(\Sigma_{HT}^{hol})^0$ , as a function of the  $y$  rapidity of the pion at the transverse momentum of the pion  $p_T = 16.7 \text{ GeV}/c$ , at the c.m. energy  $\sqrt{s} = 209 \text{ GeV}$ .

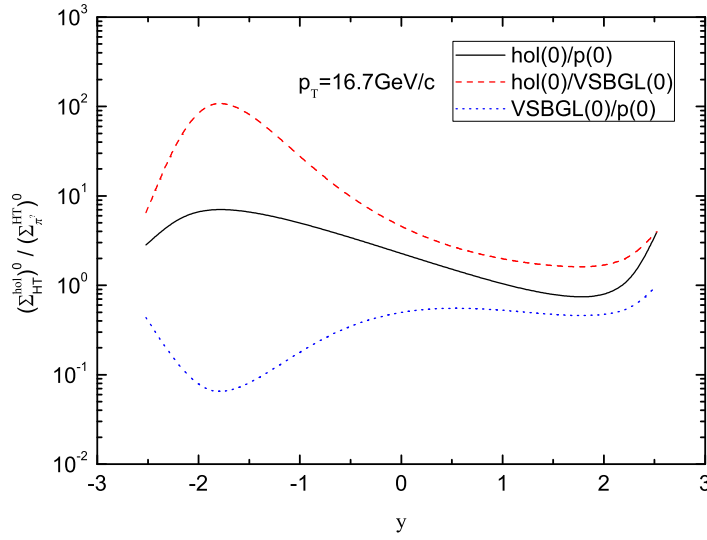


FIG. 14: Ratio  $(\Sigma_{HT}^{hol})^0 / (\Sigma_{\pi^+}^{HT})^0$ , as a function of the  $y$  rapidity of the pion at the transverse momentum of the pion  $p_T = 16.7 \text{ GeV}/c$ , at the c.m. energy  $\sqrt{s} = 209 \text{ GeV}$ .

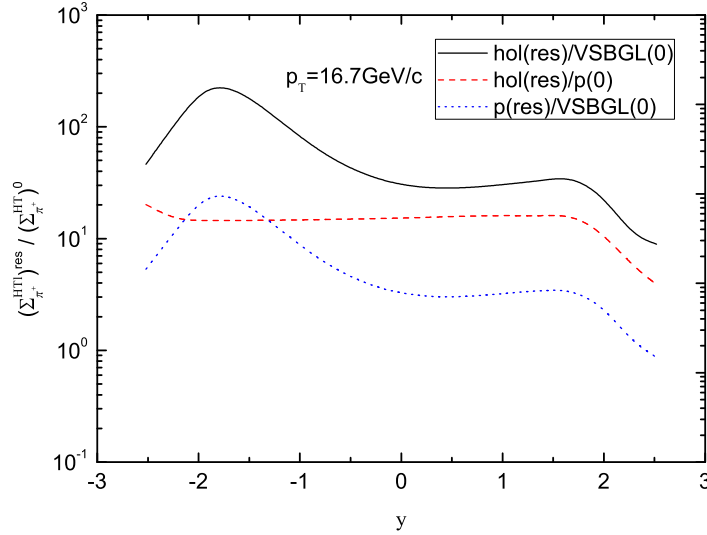


FIG. 15: Ratio  $(\Sigma_{\pi^+}^{HT})^{res} / (\Sigma_{\pi^+}^{HT})^0$ , as a function of the  $y$  rapidity of the pion at the transverse momentum of the pion  $p_T = 16.7 \text{ GeV}/c$ , at the c.m. energy  $\sqrt{s} = 209 \text{ GeV}$ .